ORIGINAL ARTICLE

Realizing time-staggered expression of nucleic acid-encoded proteins by co-delivery of messenger RNA and plasmid DNA on a single nanocarrier

Sarah S. Nasr[1,2,3,4] · Pascal Paul[1] · Brigitta Loretz[1] · Claus-Michael Lehr[1,2]

Abstract

Co-delivery of different protein-encoding polynucleotide species with varying expression kinetics of their therapeutic product will become a prominent requirement in the realm of combined nucleic acid(NA)-based therapies in the upcoming years. The current study explores the capacity for time-staggered expression of encoded proteins by simultaneous delivery of plasmid DNA (pDNA) in the core and mRNA on the shell of the same nanocarrier. The core is based on a Gelatin Type A-pDNA coacervate, thermally stabilized to form an irreversible nanogel stable enough for the deposition of cationic coats namely, protamine sulfate or LNP-related lipid mixtures. Only the protamine-coated nanocarriers remained colloidally stable following mRNA loading and could successfully co-transfect murine dendritic cell line DC2.4 with fluorescent reporter mRNA(mCherry) and pDNA (pAmCyan1). Further investigation of the protamine-coated nanosystem only, the transfection efficiency (percentage of transfected cells) and level of protein expression (mean fluorescence intensity, MFI) of mRNA and pDNA, simultaneously delivered by the same nanocarrier, were compared and kinetically assessed over 48 h in DC2.4 using flow cytometry. The onset of transfection for both nucleotides was initially delayed, with levels < 5% at 6 h. Thereafter, mRNA transfection reached 90% after 24 h and continued to slightly increase until 48 h. In contrast, pDNA transfection was clearly slower, reaching approximately 40% after 24 h, but continuing to increase to reach 94% at 48 h. The time course of protein expression (represented by MFI) for both NAs essentially followed that of transfection. Model-independent as well as model-dependent kinetic parameters applied to the data further confirmed such time-staggered expression of the two NA's where mRNA's rate of transfection and protein expression initially exceeded those of pDNA in the first 24 h of the experiment whereas the opposite was true during the second 24 h of the experiment where pDNA displayed the higher response rates. We expect that innovative nanocarriers capable of time-staggered co-delivery of different nucleotides could open new perspectives for multi-dosing, pulsatile or sustained expression of nucleic acid-based therapeutics in protein replacement, vaccination, and CRISPR-mediated gene editing scenarios.

Keywords Temporally-resolved expression · Sequential expression · Polynucleotide co-delivery · Protein expression kinetics · Transfection kinetics

✉ Sarah S. Nasr
snasr@umd.edu; sara.nasr@alexu.edu.eg;
nasrsara@hotmail.com

✉ Claus-Michael Lehr
Claus-Michael.Lehr@helmholtz-hips.de

1   Helmholtz Institute for Pharmaceutical Research Saarland (HIPS), Helmholtz Centre for Infection Research (HZI), Saarland University, Campus E8 1, 66123 Saarbrücken, Germany

2   Department of Pharmacy, Saarland University, 66123 Saarbrücken, Germany

3   Fischell Department of Bioengineering, University of Maryland, College Park, USA

4   Department of Pharmaceutics, Faculty of Pharmacy, Alexandria University, Alexandria 21521, Egypt

Introduction

Following the outbreak of the COVID-19 pandemic, the approval of mRNA-based vaccines and their mass administration with high efficiency [1–3] and safety margin in the general population [4–7], is currently accelerating the advancement of nucleic acid (NA) based therapeutic [8]. In particular major impact is expected in the fields of infectious diseases [9, 10]] and cancer [11–17], but shall also encompass hereditary and other chronic or acute health issues [8, 18, 19]. This expanding clinical application raises the demand to deliver different polynucleotide cargos simultaneously as well as to better control the kinetics of transfection and protein expression of such therapies. This may allow the optimization of the pharmacokinetics of NA-based therapeutics, same as controlled-release technologies had been successfully implemented earlier for many conventional therapeutics. To design combination NA therapies several modifications must be considered. The required modifications will most probably not only be concerned with the nucleic acid cargo's structure but also their delivery systems [20–22]. The objective of the current manuscript is to bring a specific requirement of future gene therapies and a possible approach to addressing it to light. The requirement being the co-administration of two (or more) therapeutic proteins encoding NAs on a single carrier, to a single cell, yet have them perform their therapeutic action in a time-staggered manner. The possible approach to address that is designing a nanocarrier that can effectively deliver multiple NA cargos and affect their expression in a time-staggered manner.

Many studies explored the potential possibility and benefits of co-delivering more than one polynucleotide species whether homogenous or heterogenous on a single nanocarrier [23–27]. Some of these studies demonstrated that co-loading two different mRNAs on a single nanocarrier achieved a more predictable and ratio-metric expression of the mRNA encoded proteins in line with the mRNA cargos' doses, rather than administering such mRNAs on separate nanocarriers [23, 24]. Another study by Ball et al., demonstrated the possibility of successful co-delivery of gene-encoding mRNA and gene-silencing siRNA on lipidoid-based nanocarriers, which can in the future tend to unlimited applications[26]. Meanwhile, Abbasi et al. highlighted the value of co-delivering CRISPR Cas-9 system components on a single nanocarrier by demonstrating the superior colloidal and NA shielding capacity of polyplexes co-loaded with sgRNA and CRISPR-Cas9 encoding mRNA compared to polyplexes delivering each of these components discretely [27]. On a separate note many studies have demonstrated that controlling the kinetics of expression may lead to safer more effective therapies or vaccines and while many studies have focused on exploring and characterizing the kinetics of in-vitro and in-vivo expression of different NA classes and sub-classes [28–33], hardly any studies are dedicated to manipulating and controlling the expression kinetics of co-delivered NA species through nanocarrier design. Thus, to date, the need for developing systems that can allow for the time-resolved or staggered expression of the different NA species-encoded proteins remains hardly addressed despite its demonstrated potential to be instrumental to the success of several gene therapy approaches, some of which we hereby discuss.

Prominent applications that may benefit from controlled expression kinetics of co-delivered polynucleotides may include gene editing and NA-based vaccine adjuvantation. For example, the temporal resolution of multiple NA cargo expressions may be highly relevant in the CRISPR/Cas-9-based gene editing technologies. Studies have demonstrated the superior performance of preformed sgRNA and Cas-9 Ribonucleoprotein complex compared to sgRNA and Cas-9 encoding mRNA or pDNA formats [34]. Such findings indicated that the pre-existence of Cas-9 protein at the time of the guiding sgRNA introduction into target cells was consistently associated with better gene editing performance compared to systems relying on the concurrent expression of Cas-9 and sgRNA from NA template(s) [35]. Yet the intracellular delivery of the protein Cas-9 and the sgRNA on the same nanocarrier presents a challenge due to the sheer size as well as structural heterogeneity of both cargos [36], whereas a delivery system capable of co-delivering sgRNA and Cas-9 encoding NAs that can also affect the earlier expression of Cas-9 followed by that of sgRNA could be quite valuable in such a context.

In the nucleic acid vaccination arena, several initiatives are currently advancing towards adjuvanting such vaccines through the co-delivery of immunomodulator-encoding NA cocktails along with those encoding for antigens [37–39]. Pre-expression of antigens followed by adjuvants in such scenarios ensures the development of a proper adaptive immune response towards the desired antigen, rather than tolerance or worse an autoimmune reaction that can arise from stimulation of non-antigen primed dendritic cells [40]. Hence, the kinetics and temporal resolution of expression of such immunomodulator combinations or the antigen-immunomodulator/adjuvant combination could be detrimental to the efficacy and safety of such vaccines [41].

Possible applications where time-staggered expression may also be beneficial encompass protein replacement therapies in some chronic disease scenarios. For example, a mixture of NAs encoding Insulin in a biphasic expression mode could mimic widely successful marketed formulations like Mixtard which feature mixtures of rapidly acting soluble insulin and late-acting isophane insulin, intended to reduce the frequency of administration of subcutaneous insulin

injections [42]. Using a combination of mRNA (rapid expression) and pDNA (late expression) encoding Insulin could hence be highly relevant when considering a gene-based insulin replacement therapy. Other applications may also include infertility medications such as gonadotropins which are usually administered in cyclic regimens in which follicle-stimulating hormone (FSH) analogs are administered daily through subcutaneous injection during the first two weeks of a menstrual cycle followed by a single subcutaneous injection luteinizing hormone (LH) analog injection to release the matured follicles [43], again in this scenario if a gene-based therapeutics approach is to be adopted using genes and gene delivery systems that can minimize the frequency of SC injections through time-staggered delivery and expression of FSH and LH encoding genes can be highly valuable.

To date, several studies have already compared the expression kinetics of different NA species including plasmid DNA (pDNA), Self-amplifying mRNA (sa-mRNA), modified-base mRNA, and unmodified mRNA. Where Huysmans et al. demonstrated that following in-vivo skin electroporation with equivalent masses of the aforementioned NA species in mice, sa-mRNA displayed the highest level of expression of luciferase over 4 weeks, yet pDNA was the NA species that maintained the highest level of luciferase expression during the fourth week compared to equivalent doses of sa-mRNA. pDNA also demonstrated much lower immunogenicity compared to all the other mRNA species in the study [44]. Leyman et al. have also demonstrated similar results in pigs [45]. This data indicates the potential value of pDNA in sustained-release scenarios where minimal innate immune stimulation is required. Another situation where such a feature of pDNA may prove valuable is in situations where a wash-out period is required between repeated doses of therapeutic moieties to avoid receptor oversaturation and downregulation [46, 47]. In such a situation using sa-mRNA may not be applicable due to the sustained high level of expression that could extend from days to weeks. In such a case combining non-replicating mRNA with pDNA can provide an initial high yet transient expression simulating a loading dose followed by delayed, but extended expression from pDNA simulating a maintenance dose, thus establishing a multi-dosing scenario through a single administration.

With this study, we aim to address the existing gap in research concerned with the development of gene delivery systems capable of affecting time-staggered expression of their NA-cargos. We gradually explored the variable factors influencing the co-transfection performance of a previously reported nanosystem based on protamine-coated, thermally stabilized gelatin-pDNA coacervate (P-TS-CoAc), able to also co-deliver mRNA [48]. In addition, we explored coating the pDNA-gelatin nano-coacervates with some patisiran (ONPATTRO®) like lipid cocktail. We also supplemented the study with a full factorial design model to assess the impact of key particle assembly conditions on the colloidal and co-transfectional properties of the system. Eventually and most importantly, we analyzed the co-transfection kinetics of both fluorescent protein-encoding pDNA and mRNA and showed how such nanocarrier systems could enable a time-staggered transfection and protein expression patterns of these two NAs.

Methodology

Materials

Gelatin GELITA® MedellaPro® < = 100, porcine gelatin, 228g Bloom, pharmaceutical-grade was purchased from GELITA® Deutschland GmbH, Eberbach, Germany. Protamine sulfate was purchased from Sigma-Aldrich, Darmstadt, Germany. Plasmid DNA encoding AmCyan fluorescent protein (pAmCyan1-C1) was purchased from Clontech Laboratories Inc., Mountain View, CA, USA. Subcloning Efficiency™ DH5α E. coli competent cells were purchased from Invitrogen, Thermo Fisher Scientific, Darmstadt, Germany, Qiagen EndoFree Plasmid Mega Kit was purchased from Qiagen, Hildesheim, Germany. CleanCap® mCherry mRNA was purchased from Tri-Link BioTechnologies LLC, CA, USA. Purified water was obtained from a Milli-Q water purification system (Merck, Millipore) and is referred to as MQ water.

JetMessenger (JetM) and JetPrime (JetP) were purchased from Polyplus-transfection®, Illkirch, France. Cholesterol was purchased from Sigma-Aldrich Darmstadt, Germany. DLin-MC3-DMA was purchased from MedChemExpress (New Jersey, USA), DMG-PEG2000 was purchased from and DSPC was a kind gift from Lipoid GmbH (Ludwigshafen, Germany).

Murine dendritic cell line DC2.4 was purchased from Millipore Corporation, California, USA. Cells RMPI-1640, Fetal Calf Serum (FCS), non-essential amino acids (NEAA,100X), HBSS 1X, and HEPES buffer solution(1 M) were all purchased from Gibco, Thermo Fisher Scientific, Darmstadt, Germany. β-mercaptoethanol 100X was purchased from Merck, Darmstadt, Germany.

Nanoparticle preparation

Gelatin-pDNA coacervate-based cores (CoAc) were prepared as previously reported [48]. Briefly, 3 mg mL^{-1} gelatin type A was dissolved in MQ water at 55˚C. The gelatin solution was then mixed with 100 µg mL^{-1} pAmCyan1 at a ratio of 1:1 v/v at 37˚C by vortexing to final gelatin to pAmCyan1 mass ratio of 30:1 w/w. The cores were then thermally stabilized via four cycles of heating at 55 ± 0.5 ˚C for 30 min followed by cooling at 0 ± 0.5 ˚C for 5 min

to form thermally-stabilized gelatin-pDNA coacervates (TS-CoAc) in the form of anisotropic nanogels.

As for TS-CoAc coating, two potential coating varieties were explored and compared, in addition to the previously reported protamine sulfate [48], TS-CoAc was also coated with a lipid cocktail composed of Dlin-MC3-DMA: DSPC: Cholesterol: DMG-PEG2000 in the following molar ratios (50%:10.5%:38.5%:1.5%) (Table 1).

For lipid coating, ethanolic solutions of either Dlin-MC3-DMA, DSPC, Cholesterol, DMG-PEG2000 were mixed in the aforementioned molar ratios to a final total lipid concentration of 3.56 mg mL^{-1}. The ethanolic lipid solution was mixed with TS-CoAc in sodium acetate buffer 10 mM, pH 4.2, at a final ratio of 0.3:1 v/v via vortexing, and a final gelatin to lipid mass ratio of 0.7:1 w/w.

For the preparation of LNP controls without TS-CoAc cores, an equivalent mass of the same lipid cocktail was used. Briefly, LNPs were prepared as follows, A mixture of 5µg pDNA and 1µg mRNA in MQ water was adjusted to pH = 4.2 using 10mM sodium acetate buffer. An ethanolic lipid solution composed of Dlin-MC3-DMA: DSPC: Cholesterol: DMG-PEG2000 in the following molar ratios (50%:10.5%:38.5%:1.5%) was also prepared. Both the NAs solution and the lipid solution were mixed at a ratio of 11.2:1 v/v via vortexing for 5 s. For both L-TS-CoAc and LNP, the final NP ratio was 6.

For the protamine coating of TS-CoAc to produce (P-TS-CoAc), a protamine sulfate solution in MQ water was used, at a final gelatin-to-protamine mass ratio of 4:1 w/w. A staggered herringbone micromixer was used at a mixing ratio of 1:1 v/v and a total flow rate of 2 mL.min^{-1}. Additionally a design of experiment (DOE) approach was adopted to systematically assess the impact of a varying number of thermal stabilization cycles, and mass ratio of gelatin (core): protamine (coat) content on the particle size, PDI as well as transfection efficiency and level of protein expression in DC2.4. Hence a full factorial design

(2^3) was implemented which is detailed in supplementary materials (Table S1, Table S2).

Before cell treatment particles were re-adjusted to physiological pH by mixing with HBSS to a final ratio of 2:5 v/v. mRNA surface loading to either L-TS-CoAc or P-TS-CoAc is performed 15 min before nanocarrier application to cells in transfection experiments, whereas no such step was required for LNPs as the mRNA was already core loaded during initial assembly.

Assessment of particle size, particle size distribution, and zeta-potential of different nanocarriers using Dynamic Light Scattering (DLS)

L-TS-CoAc, as well as P-TS-CoAc, were assessed for particle size, PDI, and zeta-potential using DLS (Nano-ZS, Malvern Instruments, Worcestershire, U.K.), with 4 mW He − Ne laser at a wavelength of 633 nm and a backscattering angle of 173° at 25 °C using high-resolution mode. Before coating, TS-CoAc was analyzed at a concentration of 775 µg mL^{-1} in MQ water, whereas after lipid coating L-TS-CoAc was analyzed at a concentration of 1997 µg mL^{-1} and in sodium acetate buffer of 10 mM, pH = 4.2, whereas P-TS-CoAc were analyzed at varying concentrations of 962.5, 1150 and 1550 µg mL^{-1} for P_4-TS$_\#$-CoAc, P_2-TS$_\#$-CoAc, P_1-TS$_\#$-CoAc, respectively, in MQ water, pH = 6.1. All P-TS-CoAc nanocarriers were further followed for their colloidal stability as a function of particle size and PDI over 3 weeks at 4˚C.

Comparative assessment of transfection efficiency of L-TS-CoAc, P-TS-CoAc, and LNPs in murine dendritic cell line (DC2.4)

This assessment was done to select the best-performing co-transfecting nanosystem, that could be further investigated for its capacity for time-staggered expression of the dual

Table 1 Composition and assembly conditions of mCherry and pAmCyan1 co-loaded lipid or protamine-coated thermally stabilized gelatin-pAmCyan1 coacervates

	Lipid-coated: L-TS-CoAc	Protamine-coated: P-TS-CoAc
Core composition	Thermally stabilized pDNA-Gelatin with 4 Heating cycles (TS$_4$-CoAc)	
Coat composition	Dlin-MC3-DMA:DSPC: Cholesterol: DMG-PEG2000 (50%:10.5%:38.5%:1.5%)*	Protamine sulfate (protamine: gelatin = 1:4 w/w)
Core-loaded NA	pDNA (pAmCyan1)	
Surface-loaded NA	mRNA (mCherry)	
pDNA/mRNA ratio (w/w)	5:1	
NP Ratio (w/o gelatin core)	6	na**
Assembly technique	Vortex mixing	Microfluidic meander chip

*Molar ratios

**Given the heterogeneous molecular weight range of the protamine sulfate component, the calculation of the NP ratio was not applicable

NA cargo. In brief, the transfection efficiencies and protein expression capacities of P-TS-CoAc and L-TS-CoAc were assessed against LNPs in dendritic murine cell lines (DC2.4). Briefly, cells were initially seeded at a density of 50,000 cell/well in 24 well plates and allowed 48 h in RPMI-1640 supplemented with FCS (10% v/v), HEPES (1%), NEAA (1%), β-mercaptoethanol (0.0054%)- further referred to as DC2.4 culture medium at 37 °C and 5% CO_2 to reach approximately 80% confluence. The cells were incubated with either L-TS-CoAc, P-TS-CoAc, or LNPs in OptiMEM at concentrations equivalent to 5 μg pAmCyan1 and 1 μg mCherry per well, under shaking at 250 RPM and 37 °C for 6 h. Then particle samples were removed, cells were washed twice with HBSS, fed with fresh full medium, and further incubated for 36 h at 37 °C and 5% CO_2. Either JetM or JetP commercial transfection reagents specialized for mRNA and pDNA, respectively, were used as dual transfection tools for comparison. Where either JetM or JetP was combined with both pDNA and mRNA as per the manufacturer's protocol at final NA doses equivalent to L-TS-CoAC, P-TS-CoAc, and LNPs (5 μg pDNA, 1 μg mRNA). Dose calculation for P-TS-CoAc was based on entrapment efficiency results (Figure S2) ($97.8 \pm 1.1\%$ and $100.1 \pm 0.4\%$ for mRNA and pDNA, respectively), the same values could not be obtained for L-TS-CoAc due to poor colloidal stability of the system. Eventually, cells were detached at 36 h using Trypsin/EDTA, washed twice in HBSS, fixed using 4% paraformaldehyde, and flow-cytometrically analyzed (BD LSRFortessaTM Cell Analyzer Biosciences, Heidelberg, Germany) for pAmCyan1 and mCherry transfection efficiency on AmCyan1 and PE-Texas red channels, respectively. Data were analyzed using Flowjo version 10.8.0.

Flow-cytometric assessment of the kinetics of expression of pDNA and mRNA following DC2.4 treatment with P-TS-CoAc

To assess the kinetics of mCherry and pAmCyan1 expression in DC2.4 following P-TS-CoAc treatment, P-TS-CoAc was selected based on its co-transfection performance relative to L-TS-CoAc and LNPs (Fig. 2). Cells were cultured as previously described and then treated with the P-TS-CoAc at t = 0 h, and up to 6 h. Seven predetermined time points were selected for sample collection and assessment of transfection at 0 h, 1 h, 3 h, 6 h, 24 h,33 h and 48 h post-particle treatment. Given that flow cytometric assessment is an endpoint readout, separate but parallel samples were used for the measurement of the respective time points. As for sample collection at time points of 6 h or less, the particle treatment was removed and cells detached and analysed either at 0 h, 1 h, 3 h, or 6 h post-initial treatment. Meanwhile, for samples remaining in culture past 6 h, the particle treatment was removed at 6 h, samples washed, further incubated in DC2.4 medium then harvested for analysis at 24 h,33 h, or 48 h. All samples were harvested and flow cytometrically analysed as previously described.

Statistical analysis

Graph Pad Prism 8 for Windows (Version 8.01, Graph-Pad Software Inc.) was used for data analysis. Data were generally presented as the mean of individual values, with standard deviation indicated by the error bars. (N) equals the number of experiments, (n) equals the number of technical replicates per sample in a single experiment. For longitudinal experiments, two-way ANOVA followed by Tukey's post hoc test was used. For fixed time point experiments one-way ANOVA was followed by Tukey's post hoc test was used. Data were considered statistically significant at a level of significance of $p < 0.05$ (* $p < 0.05$, ** $p < 0.01$, *** $p < 0.001$, and **** $p < 0.0001$).

Results and discussion

Particle characteristics of protamine-coated thermally stabilized gelatin-pDNA coacervates (P-TS-CoAc) and Lipid coated gelatin-pDNA coacervates (L-TS-CoAc)

Two particle compositions were proposed, both featuring a core–shell structure in which the thermally stabilized Gelatin-pDNA coacervate serves as core, whereas the shell is varied between either protamine sulphate or a lipid cocktail featuring the same lipid composition and molar ratios as patisiran. Patisiran is an siRNA-LNP formulation, and was the first LNP delivered RNA therapy to be approved by FDA in 2018 for the treatment of hereditary transthyretin-mediated amyloidosis in 2018 under the commercial name ONPATTRO® [49]. The composition of LNP employed in ONPATTRO® later served as the gold standard upon which LNPs later adopted for mRNA vaccine delivery were fashioned [50].

DLS results provided the first evidence for the successful coating of TS-CoAc with either protamine sulfate (P-TS-CoAc) or the lipid mixture (L-TS-CoAc). Both P-TS-CoAc and L-TS-CoAc displayed increased particle diameters of 257.3 ± 3.3 nm and 273.3 ± 3.2 nm, respectively in comparison to the non-coated TS-CoAc (168 ± 5.8 nm) (Fig. 1-a), and the same was observed for PDI (Fig. 1-b). For P-TS-CoAc the core–shell structure was previously confirmed using TEM [48]. A reversal in zeta-potential from a slightly negative value of -3.6 ± 0.8 for TS-CoAc to either 14.9 ± 0.6 For L-TS-CoAc or 8.3 ± 0.5 for P-TS-CoAc (Fig. 1-c) provides further evidence for the successful cationic coat deposition for both nanocarriers. Both particle size distribution
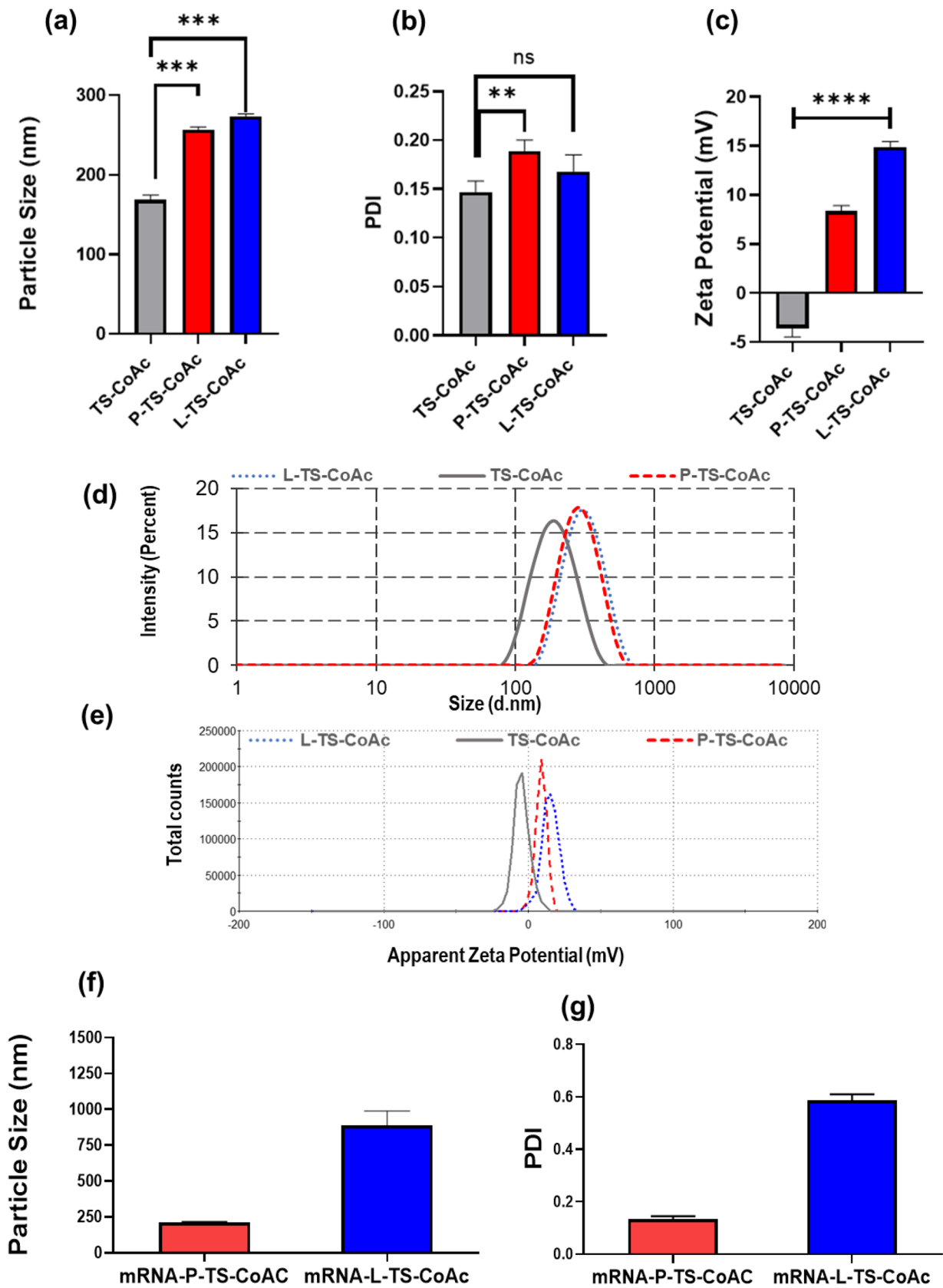
◄Fig. 1 Dynamic light scattering assessment of (**a**) particle size (nm) (**b**) PDI and (**c**) zeta-potential (mV) of either uncoated (TS-CoAc) (grey), protamine sulfate coated (P-TS-CoAc) (red) and lipid coated (L-TS-CoAc) (blue), thermally stabilized gelatin-pAmCyan1 coacervate. (**d**) Particle size distribution by the intensity of TS-CoAc, P-TS-CoAc, and L-TS-CoAc. (**e**) Apparent zeta-potential distribution of TS-CoAc, P-TS-CoAc, and L-TS-CoAc (**f**) Particle size (nm) of mRNA loaded P-TS-CoAc (red), L-TS-CoAc (blue). (**g**) PDI of mRNA loaded P-TS-CoAc (red), L-TS-CoAc (blue)

(high-resolution measurement mode) (Fig. 1-d), as well as zeta-potential (Fig. 1-e), showed monophasic peaks for all particles, indicating a still homogenous population of coated TS-CoAc.

Yet following mRNA loading only the protamine-coated nanosystem maintained its particle size and PDI comparable to their values before mRNA loading and within acceptable limits, while the lipid-coated system showed a considerable increase in both particle size (Fig. 1-f) and PDI (Fig. 1-g). This increase in size and PDI of L-TS-CoAc could indicate the dissociation of the nanosystem and potential disruption of the lipid coating to form alongside the original system an inhomogeneous subpopulations of predominantly lipid-based mRNA carriers. We hypothesize that, L-TS-CoAc became disrupted following the addition of mRNA to the system due to the much lower affinity of the lipid monomeric components to the anionic surface of gelatin-pDNA coacervate than that of a polycation in this case protamine. Protamine's superior affinity to the core's surface allows it to efficiently load mRNA upon its introduction to P-TS-CoAc without detaching from the coacervate surface, as evidenced by the maintained colloidal stability of the system.

Further factorial assessment of the impact of varying the number of thermal stabilization cycles of the pDNA-gelatin core as well as the protamine-to-gelatin mass ratio on the particle size and PDI (Table S1, Table S2), demonstrated that neither factor significantly affected the colloidal properties of the system (Figure S3).

It is also worth noting that preliminary attempts to load mRNA rather than pDNA within the Gelatin core have demonstrated that mRNA is unfit for this mode of encapsulation as its coacervate with gelatin immediately dissociated upon exposure to the thermal stabilization technique that was conversely well tolerated by pDNA (Figure S1).

In-vitro transfection performance of L-TS-CoAc, P-TS-CoAc, and LNPs in murine dendritic cell line (DC2.4)

This experiment was aimed at the comparative assessment of the co-transfection performance of a lipid-coated TS-CoAc against the previously reported protamine-coated one [48]. Where P-TS-CoAc had already displayed superior co-transfection capacities of fluorescent reporters encoding

mCherry and pAmCyan1 compared to an equivalent mass of protamine alone, simply complexed with equivalent doses of the fluorescent reporters. That experiment indicated some degree of merit of the core–shell arrangement to the desired co-transfection [48]. An observation we have resorted to a potential trojan horse-like effect, where the core–shell arrangement allows a considerable mass of pDNA to be occluded in the coacervate core rather than interacting with coating protamine, hence allowing the system to operate at an apparently higher NP ratio by sparing more cationic moieties from protamine to affect endosomal escape of the carrier [51]. Hence, given the established superiority of ionizable lipid, helper lipid, cholesterol, and pegylated lipid combinations in siRNA and mRNA delivery in clinical settings [20], we aimed to further explore the capacity of a lipid-coated against a protamine-coated system.

Results demonstrated that in terms of transfection efficiency, 36 h following treatment application to DC2.4, JetM, LNPs, L-TS-CoAc, and P-TS-CoAc could all achieve a statistically significant enhancement in % of cells expressing mCherry (%transfection efficiency) (Fig. 2-b) as well as, the protein expression level (MFI) (Fig. 2-c) compared to untreated control. While no statistically significant difference in mCherry transfection efficiency between P-TS-CoAc, L-TS-CoAc, and JetM could be observed, LNP demonstrated significantly higher transfection efficiency of mCherry compared to both P-TS-CoAc and JetM. Regarding the levels of mCherry expression, all the applied treatments resulted in a statistically significant enhancement in mCherry expression level compared to untreated control.

On the other hand, L-TS-CoAc and P-TS-CoAc showed no statistically significant difference in mCherry expression levels from one another. This could indicate comparable endosomal escape capabilities of protamine for P-TS-CoAc [52], and the ionizable [53, 54] and helper lipid [55] components of L-TS-CoAc [3], since endosomal escape is the rate-limiting step of mRNA expression [56–58].

As for pAmCyan1 transfection efficiency, none of the treatments except for P-TS-CoAc demonstrated any statistically significant improvement in pAmCyan1 transfection compared to the untreated control. As for levels of pAmCyan1 expression, P-TS-CoAc was the only treatment that produced a statistically significant pAmCyan1 expression level compared to untreated control, with a 3.4-fold increase in MFI, thus making P-TS-CoAc the only successful system for simultaneous transfection with mRNA and pDNA, highlighting the unique co-transfectional capacity of this nanosystem.

Neither L-TS-CoAc nor LNP could produce an effective expression of their pDNA cargos. The data is in line with what has been previously demonstrated by Kulkarni et al. for Dlin-MC3-DMA and DSPC-based LNPs for pDNA delivery [59]. In general, for LNPs, pDNA, and mRNA transfection

Fig. 2 Flow-cytometric analysis of the impact of varying coat structur e on the co-transfectional performance of TS-CoAc for pDNA (pAmCyan1) and mRNA (mCherry). **a** Shift in flourescence intenstity of DC2.4 36h following treatement with different samples and controls on PE-Texas red channel for mCherry treatment (left) and AmCyan channel for pAmCyan1 (right). **b** Transfection efficiency of DC2.4 with either mCherry (red) or pAmCyan1 (green) 36h following treatement with different samples with equivalent doses of 5µg pAmCyan1 and 1µg mRNA, data is displayed as mean ±SD (n=3), dotted line represents background signal of untreated control. **c** Mean flourescence intensity (MFI) of mCherry (red) or pAmCyan1 (green) encoded protens in DC2.4 following treatment with different samples with equivalent doses of 5µg pAmCyan1 and 1µg mRNA. Data are displayed as mean±SD (n =3), dotted line represents background MFI of untreated control. **** $p <$ 0.0001; *** $p <$ 0.001; ** $p <$ 0.01; ns = not significant
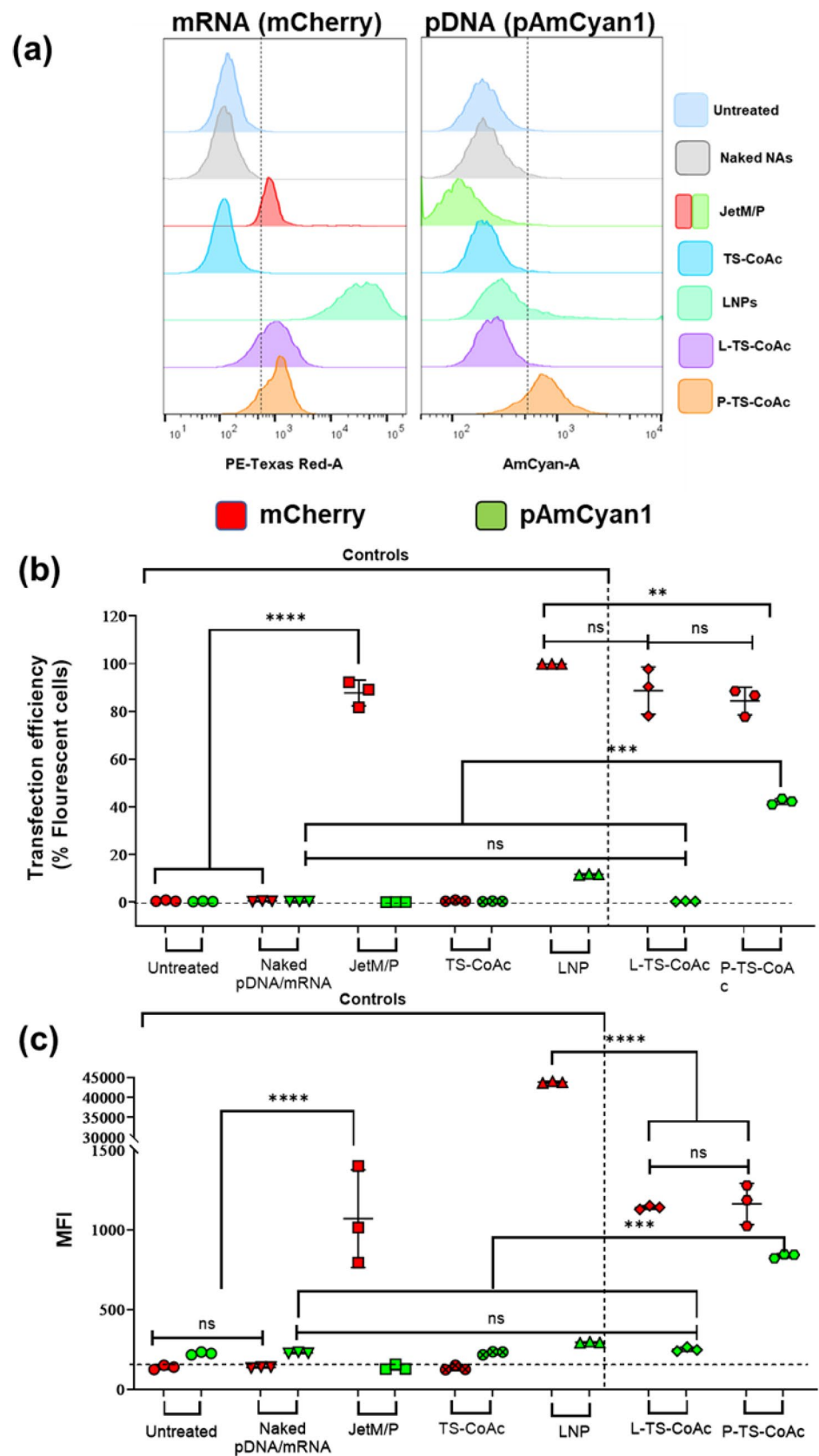
can be improved by using unsaturated helper lipids [59], which have also been reported as more efficient for mRNA transfection [60]. Eventually, however, DSPC was incorporated in all the commercial mRNA transfection systems, possibly due to outperforming unsaturated counterparts in these particular LNP formulations [3] or for stability reasons.

The presence of nuclear translocation factors is essential for successful pDNA transfection. Both LNPs and L-TS-CoAc lacked any nuclear translocation sequences, which could be the main reason for their poor pDNA transfection. On the other hand, P-TS-CoAc was uniquely capable of successful co-transfection with pDNA- alongside mRNA- mainly due to the nuclear translocation properties of protamine rendered by four nuclear translocation-like signals present in its structure [61, 62]. To conclude, upon comparing the co-transfectional capacity of P-TS-CoAc to either L-TS-CoAc, LNPs, JetM, or JetP, P-TS-CoAc showed a unique potential for incurring successful simultaneous transfection of DC2.4 with both the pDNA and mRNA cargos (Fig. 2-a).

Further factorial assessment of the impact of varying the number of thermal stabilization cycles of the pDNA-gelatin core as well as the protamine to gelatin mass ratio on the in-vitro transfection and protein expression performance of the particles (Table S1, Table S2), demonstrated that neither factor significantly affected transfection efficiency or protein expression capacity of the different particles (Figure S5). Yet further assessment of the impact of varying the aforementioned particle assembly conditions on P-TS-CoAc's cytotoxicity demonstrated that P-TS-CoAc assembled using the least number of thermal stabilization cycles and highest gelatin: protamine mass ratios showed the lowest cytotoxicity and demonstrated cell viability exceeding 98% (Figure S4).*Assessment of the kinetics of expression of pDNA and mRNA following DC2.4 treatment with P-TS-CoAc.*

Following the factorial analysis of varying P-TS-CoAc assembly conditions on transfection efficiency and level of protein expression in DC2.4, we proceeded to assess the time-resolved expression of mCherry and pAmCyan1 in DC2.4 over 48 h (Fig. 3-a). P_4-TS_4-CoAc was selected for this experiment given its favorable assembly conditions, cytocompatibility (Figure S4) as well as high pAmCyan1 and mCherry transfection efficiencies in DC2.4 48 h following original particle treatment (Fig. 2-b, Figure S5). JetM was used as a positive control for mRNA transfection, whereas JetP was used as a positive control for pDNA transfection.

During the first 6 h following P-TS-CoAc application, no statistically significant increase in transfection efficiency could be detected for either mCherry or pAmCyan1 (Fig. 3-a) using P-TS-CoAc as opposed to JetM and JetP, which both showed an early and significant enhancement in mRNA and pDNA transfection, respectively. After 24 h, the transfection efficiency of mRNA in terms of the percentage of fluorescent

cells had already reached a maximum of 91.9% $\pm$ 1.15 and later decreased slightly to 89.3% $\pm$ 2.5 at 33 h and then continued to increase reaching 99.5% $\pm$ 0.2 at 48 h (Fig. 3-a). On the other hand, pDNA expression was delayed and only reached approximately half the transfection efficiency of mRNA at 24 h with 42.5% $\pm$ 2.5, but even continued to increase to 54.63% $\pm$ 2.95 at 33 h, eventually reaching 94.4% $\pm$ 3.16 at 48 h. Conversely, the transfection efficiencies of both JetM and JetP plateaued and even decreased slightly > 6 h incubation time following application. Additionally, the transfection efficiency peaked following 24h JetM treatment and 48h post P-TS-CoAc treatment indicating sustained transfection using P-TS-CoAc (Table 3).

In terms of protein expression levels, a time-resolved expression of the two nucleic acid cargos mCherry and pAmCyan1 could also be observed in DC2.4 following P-TS-CoAc application (Fig. 3-b). A detectable statistically significant increase in the level of mCherry expression could be observed as early as 3 h after P-TS-CoAc application, while no such detectable expression could still yet be observed for pAmCyan1 at the same time point(Figure S6-b). The first discernible expression of AmCyan1 was yet to follow at 6 h (Figure S6-b). Both expression levels of mRNA and pDNA continued to increase through 33 h and 48 h post-application. On the contrary, JetM displayed an initially very strong expression of mRNA at 6 h which continued to gradually decrease at later time points. Protein expression from mRNA using JetM peaked at 6h post-treatment, whereas it peaked at 48h following P-TS-CoAc treatment. Meanwhile, JetP displayed overall very low expression levels of pDNA compared to P-TS-CoAc.

In summary, such transfection and protein expression kinetics are indicative of the capacity of P-TS-CoAc to distinctively affect time-staggered expression profiles of both its NA cargos, represented by the early expression of mRNA and delayed and prolonged-expression from pDNA.

To perform a more detailed quantitative comparison of the transfection and protein expression kinetics of mRNA and pDNA delivered by the various treatments, we explored several approaches.

A first quantification is possible by comparing the overall magnitude of transfection or protein expression calculated as the area under the curve AUC) for the transfection efficiency vs. time curve (Fig. 3-a) denoted as AUC_{tf} over the 48h duration of the in-vitro transfection experiment. Analogously, AUC for the Mean fluorescence intensity vs. time curve (Fig. 3-b) denoted as AUC_{pe} represents the overall magnitude of protein expression (or NA translation) achieved by a treatment over the 48h duration of the in-vitro transfection experiment.

To follow the timelines of transfection and protein expression of mRNA and pDNA applied using the different treatments we used three different approaches:

Fig. 3 In-vitro transfection and protein expression kinetics of mCherry (mRNA, 1μg) and pAmCyan1 (pDNA, 5 μg) in DC.4 over 48h, following their application using P-TS-CoAc (mRNA and pDNA)), JetM (mRNA only) or JetP (pDNA only) application. **a** % cells expressing fluorescent reporter protein from mCherry (red) and pAmcyan1(green) in DC2.4 over time up to 48h following P-TS-CoAc application (solid lines) compared to commercial controls (dashed lines). **c** Level of mCherry or AmCyan expression mCherry (red) and pAmcyan1 (green) in DC2.4 over time up to 48h following P-TS-CoAc application (solid lines) compared to commercial controls JetM and JetP (dashed lines). Grey dotted lines represent the background signal for TE% or MFI of untreated controls. Levels of significance of the statistical difference between mCherry and pAmCyan-1 expression from P-TS-CoAc at similar time points are indicated by black asterisks (*). Data are displayed as mean $\pm$SD (N=1, n=3), **** $p<0.0001$; *** $p<0.001$; ** $p<0.01$, * $p<0.05$; ns = not significant
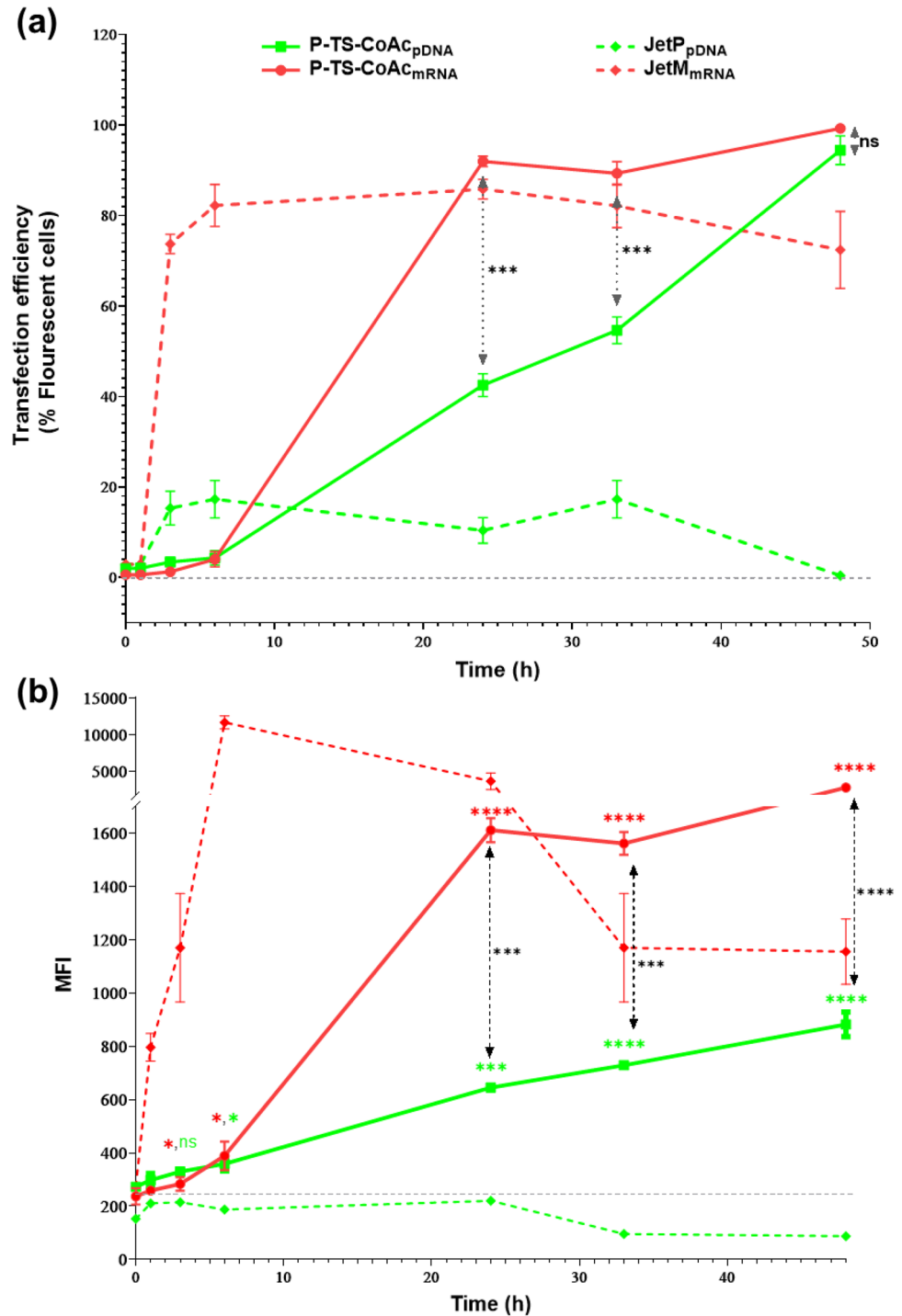
-The first parameter used for comparison was the time points (in hours) at which 50% of the maximum transfection or protein expression was achieved by a given treatment. These parameters are denoted as $T(tf)_{1/2}$ and $T(pe)_{1/2}$, respectively.

-The second, somewhat more comprehensive comparison, which takes the time course into consideration independent of any specific kinetic model is based on statistical moment analysis. It had been elaborated and applied to describe drug release from microcapsules by Brockmeier [63, 64]. For this purpose, we calculated the Mean Transfection Time (MTT) and Mean Protein expression Time (MPT) as depicted in (Figure S7-a), where;

$$MTT = \frac{ABC_{tf}}{Maximum\ transfection\ efficiency\%} \quad (1)$$

$$MPT = \frac{ABC_{pe}}{Maximum\ Mean\ flourscence\ intensity} \quad (2)$$

-The third approach to make quantitative comparisons of the transfection and protein expression kinetics followed the concept proposed earlier by Leonhardt et al. [31]. Based on slope calculation of straight lines connecting different points on the curve (Fig. 3, Figure S7-b) we could calculate the response rate coefficients between these time points (Table 2). By normalizing the slope to the number of NA molecules the obtained rate constant may be interpreted as a second-order rate constant. Such order of the rate equation would thus account for the mutual contribution of both mRNA and pDNA to each other's rate of transfection or protein expression through competing for the same cellular uptake mechanisms and protein expression machinery. Additionally, such normalization to NA dose provides a better comparison of the transfection and protein expression rates per molecule of mRNA and pDNA co-delivered on a single nanocarrier in different doses. Following this approach we could calculate response rate coefficients for either transfection K_{tf} (Table 1, Eq. 3) or protein expression K_{pe} (Table 1, Eq. 7), these response rate coefficients were calculated for initial (0h-24h) (Table 1, Eq. 5, Eq. 9), terminal (24h-48h) (Table 1, Eq. 6, Eq. 10), and overall (0h-48h) (Table 1, Eq. 4, Eq. 8), time range of the experiment as detailed in (Table 1, Figure S7).

Table 2 shows the results of the quantitative comparisons. The transfection and protein expression efficacy of the different treatments can be appreciated by the AUC. For mRNA delivered by JetM, the AUC_{tf} was 1.24 fold that of P-TS-CoAc. For pDNA, however, the AUC_{tf}, achieved with P-TS-CoAc was 3.36-fold larger than for JetP. Comparing the protein expression achieved by the different treatments it was observed that the overall mRNA expression represented by AUC_{pe}) was superior in the case of JetM to P-TS-CoAc. As for pDNA, the overall magnitude of protein expression by pDNA indicated by AUC_{pe} was far superior in the case

of P-TS-CoAc, which demonstrated an AUC_{pe} of 8.67 folds that of JetP.

The kinetics of transfection and protein expression from NAs delivered using P-TS-CoAc indicate that the expression of the two reporter proteins from the two different NA cargos occurs in a time-staggered manner in which protein expression from mRNA precedes that from pDNA. Protein expression for mRNA delivered by P-TS-CoAc was faster, reaching $T(pe)_{1/2}$ at 20.7h, whereas pDNA when delivered by the same treatment reached $T(pe)_{1/2}$ at 31.8 h. Similar trends were also observed for the time course of the transfection efficiency $T(tf)_{1/2}$.

The model-independent mean-time parameter for protein expression also showed time staggered Mean Protein Expression Times (MPT) of 42.3 h for mRNA and 45.4 h for pDNA co-delivered on P-TS-CoAc. The same was observed also for the Mean Transfection Times (MTT) (Table 3), which was16.9h for mRNA and 28.1h for pDNA delivered using P-TS-CoAc. Comparing MPT and MTT values for P-TS-CoAC delivered mRNA and pDNA to JeTM and JetP delivered ones, a general sustainment in transfection and protein expression is observed for P-TS-COAc delivered mRNA, while for pDNA the opposite is true, where both transfection and protein expression tend to come earlier for P-TS-CoAc delivered pDNA.

The model-dependent response rate kinetics of protein expression from mRNA K_{pe}(Table 3), demonstrated that the overall protein expression rate coefficient of mRNA encoded reporter protein for P-TS-CoAc $K_{pe\ (0h-48h)}$ was approximately 2.65 folds that of JetM. Meanwhile, the protein expression rate coefficient during the first 24h of the experiment $K_{pe\ (0h-24h)}$ for JetM exceeded that of P-TS-CoAc by approximately 2.5 folds. During the 2nd half of the experiment, $K_{pe\ (24h-48h)}$, for P-TS-CoAc continued to have a positive value indicating a continuation in the expression of the reporter protein exceeding its degradation. Simultaneously, the rate of reporter protein expression by JetM declined below its level of degradation as indicated by the negative value of $K_{pe\ (24h-48h)}$.

Similarly all protein expression rate coefficients ($K_{pe\ (0h-48h)}$, $K_{pe\ (0h-24h)}$, $K_{pe\ (24h-48h)}$) for pDNA encoded reporter protein were inferior in the case of JetP to

Table 2 Transfection and protein expression rate coefficients

	Transfection rate coefficient(s) (k_{tf})	Protein expression rate coefficient(s) (k_{pe})
General formula	$k_{tf(t_1-t_2)} = \frac{TE\%_{t2}-TE\%_{t1}}{(t_2-t_1)*number\ moles\ of\ NA}$ (3)	$k_{pe(t_1-t_2)} = \frac{MFI_{t2}-MFI_{t1}}{(t_2-t_1)*number\ moles\ of\ NA}$ (7)
Overall rate coefficient (0h-48h)	$k_{tf(0h-48h)} = \frac{TE\%_{48h}-TE\%_{0h}}{48h*number\ moles\ of\ NA}$ (4)	$k_{pe(0h-48h)} = \frac{MFI_{48h}-MFI_{0h}}{48h*number\ moles\ of\ NA}$ (8)
Rate coefficient for 1st 24h of experiment (0h-24h)	$k_{tf(0h-24h)} = \frac{TE\%_{24h}-TE\%_{0h}}{24h*number\ moles\ of\ NA}$ (5)	$k_{pe(0h-24h)} = \frac{MFI_{24h}-MFI_{0h}}{24h*number\ moles\ of\ NA}$ (9)
Rate coefficient for 2nd 24h of experiment (24h-48h)	$k_{tf(24h-48h)} = \frac{TE\%_{48h}-TE\%_{24h}}{24h*number\ moles\ of\ NA}$ (6)	$k_{pe(24h-48h)} = \frac{MFI_{48h}-MFI_{24h}}{24h*number\ moles\ of\ NA}$ (10)

MFI Mean Fluorescence intensity, *TE%* Transfection efficiency, *NA* Nucleic acid (mRNA or pDNA)

Table 3 Kinetic parameters of transfection and protein expression of mRNA and pDNA in DC2.4 following treatment with P-TS-CoAc, JetM or JetP

	AUC_{tf} (h)	MTT (h)	$T(tf)_{1/2}$ (h)	$K_{tf(0h-48h)}*10^{11}$ $(h^{-1}.mol^{-1})$	$K_{tf(0h-24h)}*10^{11}$ $(h^{-1}.mol^{-1})$	$K_{tf(24h-48h)}*10^{11}$ $(h^{-1}.mol^{-1})$	AUC_{pe} (h)	MPT (h)	$T(pe)_{1/2}$ (h)	$K_{pe(0h-48h)}*10^{11}$ $(h^{-1}.mol^{-1})$	$K_{pe(0h-24h)}*10^{11}$ $(h^{-1}.mol^{-1})$	$K_{pe(24h-48h)}*10^{11}$ $(h^{-1}.mol^{-1})$
JetM$_{mRNA}$	3741±90.2	10.6	2.08	4.7	11	-1.8	198,779±14,232	31.0	5.37	64	470	-340
JetP$_{pDNA}$	576.6±59.8	42.4	1.97	-0.29	1.7	-2.3	7674±204.0	47.3	31.8	-7.5	0.0016	-31
P-TS-CoAc$_{mRNA}$	3105±30.18	16.9	15.23	6.7	12	0.99	66,596±779.2	42.3	20.7	170	190	160
P-TS-CoAc$_{pDNA}$	1995±45.7	28.1	27.7	11	9.2	12	29,249±464.2	45.4	31.8	710	87	55

AUCtf magnitude of overall transfection rate, *MTT* Mean transfection time, *T(tf)max* maximum transfection time, *T(tf)1/2* 50% of maximum transfection rate time-point, *Ktf(0h-48h)* Transfection rate coefficient over 48h post treatment, *Ktf(0h-24h)* Transfection rate coefficient between 0h-24h post treatment, *Ktf(24h-48h)* Transfection rate coefficient between 24h-48h post-treatment, *AUCpe* magnitude of overall protein expression, *MPT* Mean protein expression time, *T(pe)max* maximum protein expression time, *T(pe)1/2* 50% of maximum protein expression time-point, *Kpe(0h-48h)* Protein expression rate coefficient over 48h post treatment, *Kpe(0h-24h)* Protein expression rate coefficient between 0h-24h post treatment, *Kpe(24h-48h)* Protein expression rate coefficient between 24h-48h post-treatment

P-TS-CoAc across the entire timeline of the experiment (Table 3).

Upon comparing P-TS-CoAc's protein expression rate coefficients $K_{pe\,(0h-48h)}$, $K_{pe\,(0h-24h)}$, and $K_{pe\,(24h-48h)}$, for both mRNA and pDNA (Table 3), we find that they were generally superior in the case of mRNA compared to pDNA.

Yet, with regards to mRNA transfection kinetics, the overall transfection rate coefficient $K_{tf\,(0h-48h)}$ of DC2.4 with P-TS-CoAc was 1.42 fold that with jetM, despite JeTM possessing a higher AUC_{tf}. During the 1st 24h of the experiment, both P-TS-CoAc and JetM had comparable transfection rate coefficients of $1.2E+12$ and $1.1E+12$, respectively (Table 3). Yet, the bulk of the superior performance of P-TS-CoAc in comparison to JetM in terms of transfection rate occurred during the 2nd 24h of the experiment, where JetM experienced a steep dip in its transfection rate indicated by the negative value of its $K_{tf\,(24h-48h)}$. P-TS-CoAc, despite experiencing a significant decline to its transaction rate coefficient still maintained a progressive increase in transfection rates over the 2nd 24h of the experiment, as indicated by the positive value of its transfection rate coefficient $K_{tf\,(24h-48h)}$.

In a similar fashion to the protein expression kinetics, the rate constants $K_{tf\,(0h-48h)}$, $K_{tf\,(0h-24h)}$, $K_{tf\,(24h-48h)}$ illustrate that this process was much faster in the case of P-TS-CoAc compared to JetP, going parallel with a higher transfection rate of P-TS-CoAc throughout the entire timeline of the experiment.

Comparing the transfection rate coefficients of mRNA and pDNA delivered using P-TS-CoAc, a crucial observation was that while the transfection rate coefficient $K_{tf\,(0h-24h)}$ of mRNA exceeded that of pDNA during the 1st 24h of the experiment by 1.3 folds, the opposite was true for the second 24h of the experiment in which the transfection rate coefficient $K_{tf\,(24h-48h)}$ of pDNA was 13 folds that of mRNA. This observation further demonstrated the time-staggered transfection pattern in which mRNA transfection precedes that of pDNA.

Conclusions

The current study demonstrated the potential of protamine-coated, thermally stabilized gelatin-pDNA complex coacervate (P-TS-CoAc), as a nanocarrier system suitable for co-delivery and time-staggered expression of pDNA and mRNA. This was not possible with either the widely used commercial transfection agents JetPrime and JetMessenger or with clinically established lipid nanoparticles (LNP) currently considered as mRNA delivery gold standard. By comparing the kinetics of transfection and protein expression for each of the co-delivered NAs in more detail, an interesting feature of the reported nanosystem is observed, namely its capacity to instigate time-staggered transfection and protein expression for the two simultaneously delivered NA

cargos. While mRNA produced an early, strong, and transient expression, pDNA produced a delayed yet prolonged expression. The possibility to realize different expression kinetics for protein-encoding polynucleotides could become useful within an NA-based vaccination context, for example, optimizing the co-delivery of NA-based antigens and adjuvants, where time resolution between antigen and adjuvant expression can strongly affect vaccine safety and efficacy. Such features can also become highly relevant in protein replacement combination or sustained therapy scenarios, as well as CRISPR-based gene editing technologies.

Declarations

Ethics Statement All experiments were authorized by the institutional research ethics committee at HIPS-HZI.

Competing interests The authors have no relevant financial or non-financial interests to disclose.

References

1. Cheng H, Peng Z, Luo W, Si S, Mo M, Zhou H, Xin X, Liu H, Yu Y. Efficacy and Safety of COVID-19 Vaccines in Phase III Trials: A Meta-Analysis. Nato Adv Sci Inst Se. 2021;9:582. https://doi.org/10.3390/vaccines9060582.

2. Verbeke R, Lentacker I, Smedt SCD, Dewitte H. The dawn of mRNA vaccines: The COVID-19 case. J Control Release. 2021;333:511–20. https://doi.org/10.1016/j.jconrel.2021.03.043.

3. Chaudhary N, Weissman D, Whitehead KA. mRNA vaccines for infectious diseases: principles, delivery and clinical translation. Nat Rev Drug Discov. 2021;20:817–38. https://doi.org/10.1038/s41573-021-00283-5.

4. Wu Q, Dudley MZ, Chen X, Bai X, Dong K, Zhuang T, Salmon D, Yu H. Evaluation of the safety profile of COVID-19 vaccines: a rapid review. Bmc Med. 2021;19:173. https://doi.org/10.1186/s12916-021-02059-5.

5. Chen M, Yuan Y, Zhou Y, Deng Z, Zhao J, Feng F, Zou H, Sun C. Safety of SARS-CoV-2 vaccines: a systematic review and meta-analysis of randomized controlled trials. Infect Dis Poverty. 2021;10:94. https://doi.org/10.1186/s40249-021-00878-5.

6. Ciapponi, A, Bardach, A, Mazzoni A, Alconada T, Anderson S, Argento FJ, Ballivian J , Bok K, Comandé D, Erbelding E, Goucher E, Kampmann B, Karron R, Munoz FM, Palermo MC, Parker EPK, Cairoli FR, Santa MV, Stergachis A, Voss G, Xiong X, Zamora N, Zaraa S, Berrueta M, Buekens PM. Safety of COVID-19 vaccines, their components or their platforms for pregnant women: A rapid review, Medrxiv. 2021;2021.06.03.21258283. https://doi.org/10.1101/2021.06.03.21258283.

7. Castells MC, Phillips EJ. Maintaining Safety with SARS-CoV-2 Vaccines, New Engl J Med. 2020;384 NEJMra2035343. https://doi.org/10.1056/nejmra2035343.

8. Damase TR, Sukhovershin R, Boada C, Taraballi F, Pettigrew RI, Cooke JP. The Limitless Future of RNA Therapeutics. Frontiers Bioeng Biotechnology. 2021;9: 628137. https://doi.org/10.3389/fbioe.2021.628137.

9. Jackson NAC, Kester KE, Casimiro D, Gurunathan S, DeRosa F. The promise of mRNA vaccines: a biotech and industrial perspective. NPJ Vaccines. 2020;5:11. https://doi.org/10.1038/s41541-020-0159-8.

10. Maruggi G, Zhang C, Li J, Ulmer JB, Yu D. mRNA as a Transformative Technology for Vaccine Development to Control Infectious Diseases. Mol Ther. 2019;27:757–72. https://doi.org/10.1016/j.ymthe.2019.01.020.

11. Beck JD, Reidenbach D, Salomon N, Sahin U, Türeci Ö, Vormehr M, Kranz LM. mRNA therapeutics in cancer immunotherapy. Mol Cancer. 2021;20:69. https://doi.org/10.1186/s12943-021-01348-0.

12. Han G, Noh D, Lee H, Lee S, Kim S, Yoon HY, Lee SH. Advances in mRNA Therapeutics for Cancer Immunotherapy: From Modification to Delivery. Adv Drug Deliv Rev. 2023;199: 114973. https://doi.org/10.1016/j.addr.2023.114973.

13. Ataş E. mRNA Based Therapeutic Strategies in Cancer Immunotherapy. J Mol Virol Immunol. 2021;1:1–7. https://doi.org/10.46683/jmvi.2020.18.

14. Kübler H, Scheel B, Gnad-Vogt U, Miller K, Schultze-Seemann W, vom Dorp F, Parmiani G, Hampel C, Wedel S, Trojan L, Jocham D, Maurer T, Rippin G, Fotin-Mleczek M, von der Mülbe F, Probst J, Hoerr I, Kallen K-J, Lander T, Stenzl A. Self-adjuvanted mRNA vaccination in advanced prostate cancer patients: a first-in-man phase I/IIa study. J Immunother Cancer. 2015;3:26. https://doi.org/10.1186/s40425-015-0068-y.

15. Zhang H, Xia X. RNA cancer vaccines: developing mRNA nanovaccine with self-adjuvant property for cancer immunotherapy. Hum Vaccines Immunother. 2021;17:2995–8. https://doi.org/10.1080/21645515.2021.1921524.

16. Lint SV, Renmans D, Broos K, Dewitte H, Lentacker I, Heirman C, Breckpot K, Thielemans K. The ReNAissanCe of mRNA-based cancer therapy. Expert Rev Vaccines. 2015;14:235–51. https://doi.org/10.1586/14760584.2015.957685.

17. Heine A, Juranek S, Brossart P. Clinical and immunological effects of mRNA vaccines in malignant diseases. Mol Cancer. 2021;20:52. https://doi.org/10.1186/s12943-021-01339-1.

18. Sahin U, Karikó K, Türeci Ö. mRNA-based therapeutics — developing a new class of drugs. Nat Rev Drug Discov. 2014;13:759–80. https://doi.org/10.1038/nrd4278.

19. Weng Y, Li C, Yang T, Hu B, Zhang M, Guo S, Xiao H, Liang X-J, Huang Y. The challenge and prospect of mRNA therapeutics landscape. Biotechnol Adv. 2020;40: 107534. https://doi.org/10.1016/j.biotechadv.2020.107534.

20. Hou X, Zaks T, Langer R, Dong Y. Lipid nanoparticles for mRNA delivery. Nat Rev Mater. 2021;6:1078–94. https://doi.org/10.1038/s41578-021-00358-0.

21. Tenchov R, Bird R, Curtze AE, Zhou Q. Lipid Nanoparticles From Liposomes to mRNA Vaccine Delivery, a Landscape of Research Diversity and Advancement. ACS Nano. 2021;15:16982–7015. https://doi.org/10.1021/acsnano.1c04996.

22. Shin MD, Shukla S, Chung YH, Beiss V, Chan SK, Ortega-Rivera OA, Wirth DM, Chen A, Sack M, Pokorski JK, Steinmetz NF. COVID-19 vaccine development and a potential nanomaterial path forward. Nat Nanotechnol. 2020;15:646–55. https://doi.org/10.1038/s41565-020-0737-y.

23. Zhang H, Bussmann J, Huhnke FH, Devoldere J, Minnaert A, Jiskoot W, Serwane F, Spatz J, Röding M, Smedt SCD, Braeckmans K, Remaut K. Together is Better: mRNA Co-Encapsulation in Lipoplexes is Required to Obtain Ratiometric Co-Delivery and Protein Expression on the Single Cell Level. Adv Sci. 2021;9:2102072. https://doi.org/10.1002/advs.202102072.

24. Moradian H, Lendlein A, Gossen M. Strategies for simultaneous and successive delivery of RNA. J Mol Med. 2020;98:1767–79. https://doi.org/10.1007/s00109-020-01956-1.

25. Li J, Liang X, Huang Y, Meng S, Xie R, Deng R, Yu L. Enhancement of the immunogenicity of DNA vaccine against infectious bursal disease virus by co-delivery with plasmid encoding chicken interleukin 2. Virology. 2004;329:89–100. https://doi.org/10.1016/j.virol.2004.07.033.

26. Ball RL, Hajj KA, Vizelman J, Bajaj P, Whitehead KA. Lipid Nanoparticle Formulations for Enhanced Co-delivery of siRNA and mRNA. Nano Lett. 2018;18:3814–22. https://doi.org/10.1021/acs.nanolett.8b01101.

27. Abbasi S, Uchida S, Toh K, Tockary TA, Dirisala A, Hayashi K, Fukushima S, Kataoka K. Co-encapsulation of Cas9 mRNA and guide RNA in polyplex micelles enables genome editing in mouse brain. J Control Release. 2021;332:260–8. https://doi.org/10.1016/j.jconrel.2021.02.026.

28. Phua KKL, Leong KW, Nair SK. Transfection efficiency and transgene expression kinetics of mRNA delivered in naked and nanoparticle format. J Control Release. 2013;166:227–33. https://doi.org/10.1016/j.jconrel.2012.12.029.

29. Pardi N, Tuyishime S, Muramatsu H, Kariko K, Mui BL, Tam YK, Madden TD, Hope MJ, Weissman D. Expression kinetics of nucleoside-modified mRNA delivered in lipid nanoparticles to mice by various routes. J Control Release. 2015;217:345–51. https://doi.org/10.1016/j.jconrel.2015.08.007.

30. Ligon TS, Leonhardt C, Rädler JO. Multi-Level Kinetic Model of mRNA Delivery via Transfection of Lipoplexes. PLoS ONE. 2014;9: e107148. https://doi.org/10.1371/journal.pone.0107148.

31. Leonhardt C, Schwake G, Stögbauer TR, Rappl S, Kuhr JT, Ligon TS, Rädler JO. Single-cell mRNA transfection studies: Delivery kinetics and statistics by numbers. Nanomed Nanotechnol Biol Med. 2014;10:679–88. https://doi.org/10.1016/j.nano.2013.11.008.

32. Yasar H, Biehl A, Rossi CD, Koch M, Murgia X, Loretz B, Lehr C-M. Kinetics of mRNA delivery and protein translation in dendritic cells using lipid-coated PLGA nanoparticles. J Nanobiotechnology. 2018;16:72. https://doi.org/10.1186/s12951-018-0401-y.

33. Ditto AJ, Shah PN, Gump LR, Yun YH. Nanospheres Formulated from l-Tyrosine Polyphosphate Exhibiting Sustained Release of Polyplexes and In Vitro Controlled Transfection Properties. Mol Pharm. 2009;6:986–95. https://doi.org/10.1021/mp9000316.

34. Kouranova E, Forbes K, Zhao G, Warren J, Bartels A, Wu Y, Cui X. CRISPRs for Optimal Targeting: Delivery of CRISPR Components as DNA, RNA, and Protein into Cultured Cells and Single-Cell Embryos. Hum Gene Ther. 2016;27:464–75. https://doi.org/10.1089/hum.2016.009.

35. Lin Y, Wagner E, Lächelt U. Non-viral delivery of the CRISPR/Cas system: DNA versus RNA versus RNP. Biomater Sci-Uk. 2022;10:1166–92. https://doi.org/10.1039/d1bm01658j.

36. Sioson VA, Kim M, Joo J. Challenges in delivery systems for CRISPR-based genome editing and opportunities of nanomedicine, Biomed. Eng Lett. 2021;11:217–33. https://doi.org/10.1007/s13534-021-00199-4.

37. Yang J, Arya S, Lung P, Lin Q, Huang J, Li Q. Hybrid nanovaccine for the co-delivery of the mRNA antigen and adjuvant. Nanoscale. 2019;11:21782–9. https://doi.org/10.1039/c9nr05475h.

38. Chatzikleanthous D, O'Hagan DT, Adamo R. Lipid-Based Nanoparticles for Delivery of Vaccine Adjuvants and Antigens: Toward Multicomponent Vaccines. Mol Pharmaceut. 2021;18:2867–88. https://doi.org/10.1021/acs.molpharmaceut.1c00447.

39. Hotz C, Wagenaar TR, Gieseke F, Bangari DS, Callahan M, Cao H, Diekmann J, Diken M, Grunwitz C, Hebert A, Hsu K, Bernardo M, Karikó K, Kreiter S, Kuhn AN, Levit M, Malkova N, Masciari S, Pollard J, Qu H, Ryan S, Selmi A, Schlereth J, Singh K, Sun F, Tillmann B, Tolstykh T, Weber W, Wicke L, Witzel S, Yu Q, Zhang YA, Zheng G, Lager J, Nabel GJ, Sahin U, Wiederschain D. Local delivery of mRNA-encoding cytokines promotes antitumor immunity and tumor eradication across multiple preclinical tumor models. Sci Transl Med. 2021;13:eabc7804. https://doi.org/10.1126/scitranslmed.abc7804.

40. Nam J-H, Lee J-H, Choi S-Y, Jung N-C, Song J-Y, Seo H-G, Lim D-S. Functional Ambivalence of Dendritic Cells: Tolerogenicity and Immunogenicity. Int J Mol Sci. 2021;22:4430. https://doi.org/10.3390/ijms22094430.

41. Zhu M. Immunological perspectives on spatial and temporal vaccine delivery. Adv Drug Deliver Rev. 2021;178: 113966. https://doi.org/10.1016/j.addr.2021.113966.

42. Mixtard, INN-insulin human (rDNA) - mixtard-epar-summary-public_en.pdf, (n.d.). https://www.ema.europa.eu/en/documents/overview/mixtard-epar-summary-public_en.pdf (accessed December 20, 2023).

43. Fauser BC , Patient education: Infertility treatment with gonadotropins (Beyond the Basics) - UpToDate, (n.d.). https://www.uptodate.com/contents/infertility-treatment-with-gonadotropins-beyond-the-basics (accessed December 20, 2023).

44. Huysmans H, Zhong Z, Temmerman JD, Mui BL, Tam YK, Cafferty SM, Gitsels A, Vanrompay D, Sanders NN. Expression Kinetics and Innate Immune Response after Electroporation and LNP-Mediated Delivery of a Self-Amplifying mRNA in the Skin. Mol Ther Nucleic Acids. 2019;17:867–78. https://doi.org/10.1016/j.omtn.2019.08.001.

45. Leyman B, Huysmans H, Cafferty SM, Combes F, Cox E, Devriendt B, Sanders NN. Comparison of the Expression Kinetics and Immunostimulatory Activity of Replicating mRNA. Nonreplicating mRNA, and pDNA after Intradermal Electroporation in Pigs, Mol Pharmaceut. 2018;15:377–84. https://doi.org/10.1021/acs.molpharmaceut.7b00722.

46. J. González-Maeso, S.C. Sealfon, Endocrinology, in: Chapter 5 - Hormone Signaling Via G Protein–Coupled Receptors, 2010: pp. 83–105. https://doi.org/10.1016/b978-1-4160-5583-9.00005-8.

47. Gainetdinov RR, Premont RT, Bohn LM, Lefkowitz RJ, Caron MG. Desensitization of G protein–coupled receptors and neuronal functions. Neuroscience. 2004;27:107–44. https://doi.org/10.1146/annurev.neuro.27.070203.144206.

48. Nasr SS, Lee S, Thiyagarajan D, Boese A, Loretz B, Lehr C-M. Co-Delivery of mRNA and pDNA Using Thermally Stabilized Coacervate-Based Core-Shell Nanosystems. Pharmaceutics. 2021;13:1924. https://doi.org/10.3390/pharmaceutics13111924.

49. FDA, Patisiran – Cross-Discipline Team Leader Review, (2018). https://www.accessdata.fda.gov/drugsatfda_docs/nda/2018/210922Orig1s000MultiR.pdf (accessed July 1, 2024).

50. Schoenmaker L, Witzigmann D, Kulkarni JA, Verbeke R, Kersten G, Jiskoot W, Crommelin D. mRNA-lipid nanoparticle COVID-19

vaccines: structure and stability. Int J Pharmaceut. 2021;601: 120586. https://doi.org/10.1016/j.ijpharm.2021.120586.

51. S. Nasr, Publikationen der UdS: Nanocarriers for simultaneous delivery of structurally different polynucleotides encoding antigens and adjuvants, 2022.

52. Shukla RS, Jain A, Zhao Z, Cheng K. Intracellular trafficking and exocytosis of a multi-component siRNA nanocomplex. Nanomed Nanotechnol Biology Medicine. 2016;12:1323–34. https://doi.org/10.1016/j.nano.2016.02.003.

53. Cullis PR, Hope MJ. Lipid Nanoparticle Systems for Enabling Gene Therapies. Mol Ther. 2017;25:1467–75. https://doi.org/10.1016/j.ymthe.2017.03.013.

54. Sahay G, Alakhova DY, Kabanov AV. Endocytosis of nanomedicines. J Control Release. 2010;145:182–95. https://doi.org/10.1016/j.jconrel.2010.01.036.

55. Cheng X, Lee RJ. The role of helper lipids in lipid nanoparticles (LNPs) designed for oligonucleotide delivery. Adv Drug Deliver Rev. 2016;99:129–37. https://doi.org/10.1016/j.addr.2016.01.022.

56. Lönn P, Kacsinta AD, Cui X-S, Hamil AS, Kaulich M, Gogoi K, Dowdy SF. Enhancing Endosomal Escape for Intracellular Delivery of Macromolecular Biologic Therapeutics. Sci Rep-Uk. 2016;6:32301. https://doi.org/10.1038/srep32301.

57. Erazo-Oliveras A, Muthukrishnan N, Baker R, Wang T-Y, Pellois J-P. Improving the Endosomal Escape of Cell-Penetrating Peptides and Their Cargos: Strategies and Challenges. Pharm. 2012;5:1177–209. https://doi.org/10.3390/ph5111177.

58. Teo SLY, Rennick JJ, Yuen D, Al-Wassiti H, Johnston APR, Pouton CW. Unravelling cytosolic delivery of cell penetrating peptides with a quantitative endosomal escape assay. Nat Commun. 2021;12:3721. https://doi.org/10.1038/s41467-021-23997-x.

59. Kulkarni JA, Myhre JL, Chen S, Tam YYC, Danescu A, Richman JM, Cullis PR. Design of lipid nanoparticles for in vitro and in vivo delivery of plasmid DNA. Nanomed Nanotechnol Biology Medicine. 2017;13:1377–87. https://doi.org/10.1016/j.nano.2016.12.014.

60. Kauffman KJ, Dorkin JR, Yang JH, Heartlein MW, DeRosa F, Mir FF, Fenton OS, Anderson DG. Optimization of Lipid Nanoparticle Formulations for mRNA Delivery in Vivo with Fractional Factorial and Definitive Screening Designs. Nano Lett. 2015;15:7300–6. https://doi.org/10.1021/acs.nanolett.5b02497.

61. Reynolds F, Weissleder R, Josephson L. Protamine as an Efficient Membrane-Translocating Peptide. Bioconjugate Chem. 2005;16:1240–5. https://doi.org/10.1021/bc0501451.

62. Tenkumo T, Rotan O, Sokolova V, Epple M. Protamine Increases Transfection Efficiency and Cell Viability after Transfection with Calcium Phosphate Nanoparticles. Nano Biomed. 2014;5:64–74. https://doi.org/10.11344/nano.5.64.

63. VD Brockmeier, Die Rekonstruktion der Freisetzungsprofile mikroverkapselter Arzneiformen durch den Mittelwert und die Varianz der Freisetzungszeiten Arzneimittel-Forschung/Drug Research (1981) 1746–1751. https://doi.org/10.22029/jlupub-16183

64. Brockmeier D. Mean time concept and component analysis in pharmacokinetics. Int J Clin Pharmacol Ther. 1999;37:555–61.